Lithium diffusion in the spinel phase $Li_4Ti_5O_{12}$ and in the rocksalt phase $Li_7Ti_5O_{12}$ of lithium titanate from first principles

Benedikt Ziebarth,[1,2,3,*] Markus Klinsmann,[1] Thomas Eckl,[1] and Christian Elsässer[2,3]

[1]*Corporate Sector Research and Advance Engineering, Robert Bosch GmbH, Robert-Bosch-Platz 1, 70839 Gerlingen-Schillerhöhe, Germany*

[2]*Fraunhofer Institut für Werkstoffmechanik IWM, Wöhlerstr. 11, 79108 Freiburg, Germany*

[3]*Karlsruher Institut für Technologie, Institut für Angewandte Materialien (IAM-ZBS), Engelbert-Arnold-Str. 4, 76131 Karlsruhe, Germany*

(Received 5 November 2013; revised manuscript received 7 April 2014; published 9 May 2014)

Lithium titanate (LTO) is a promising candidate as an anode material in future generations of lithium ion batteries due to its high intrinsic safety and stability. In this work, we investigate the diffusion barriers for lithium ions in two different crystal structures of LTO using the density functional theory. Our calculations show that the activation barriers vary between 0.30–0.48 eV for the spinel phase $Li_4Ti_5O_{12}$ and between 0.20–0.51 eV in the lithiated rocksalt phase $Li_7Ti_5O_{12}$. The origins of the rather broad ranges of activation energies are related to different chemical environments of the diffusion channels due to mixed occupancies of some sites in LTO. Our results reveal that the determination of lithium diffusion constants in LTO can not be carried out by using a single activation barrier. Instead, the local environment of the diffusion paths must be considered to correctly capture the variety of activation barriers. Moreover, we find the sites which have mixed occupation in LTO to trap lithium vacancies in the spinel phase. This effect is not observed in the rocksalt phase. This behavior explains the low lithium diffusivity found in experiments for lithium concentrations in the vicinity of the spinel phase.

DOI: 10.1103/PhysRevB.89.174301 PACS number(s): 66.30.−h, 31.15.A−, 82.47.Aa, 77.84.Bw

I. INTRODUCTION

In recent years, the demand of energy storage devices with large specific energy densities increased rapidly due to the ongoing increase of *electromobility*. To extend the specific energy density of lithium ion batteries even further, new electrode materials are needed to be utilized. Aside from larger capacities, also the lifetime and safety of batteries are important. One factor for a long lifetime of a battery is the mechanical robustness of the electrodes during operation, in which lithium ions are intercalated and deintercalated. These processes usually lead to volume changes in the electrodes and may result in crack formation which can damage the cell. A potential anode material for future generation of lithium ion batteries is *lithium titanate* (LTO) $Li_{4+x}Ti_5O_{12}$ ($0 \leqslant x \leqslant 3$). It exhibits only negligible volume change during lithiation since the lattice constants of the spinel $Li_4Ti_5O_{12}$ (8.3595 Å) and the lithiated rocksalt phase $Li_7Ti_5O_{12}$ (8.3538 Å) are very similar [1].

The $Li_4Ti_5O_{12}$ compound has a spinel structure with space group $Fd\bar{3}m$ [2] in which the 8*a* positions are occupied by lithium ions and 16*d* positions are shared between lithium ions and titanium ions with a ratio of 1:5. Oxygen ions occupy all 32*e* positions. Upon lithiation, lithium ions on 8*a* positions are moved to 16*c* positions while the additional lithium ions fill the remaining 16*c* vacancies and thereby change the structure of LTO from spinel to rocksalt [1].

In order to understand the process of intercalation and deintercalation, the dynamics of lithium ions in LTO needs to be understood. Ionic diffusivity in a solid is governed by thermally activated hopping of ions between interstitial positions or vacancies. The network of possible lithium sites in LTO provides a three-dimensional diffusion network through the crystal, whereas in other electrode materials the lithium motion is constrained to two dimensions, e.g., in the anode material graphite or in the cathode material CoO_2, or even to one dimension, e.g., in $LiFePO_4$ which is also a cathode material [3]. Because of the importance of lithium diffusion in LTO for its utilization in batteries, lithium diffusion properties were often investigated [4–9]. The diffusion of lithium depends on the microstructure of the material. But, even for perfect single crystals of LTO, published atomistic simulation studies using density functional theory (DFT) report different energy barriers for Li migration. The differences are of the order of the energy barrier itself, i.e., reported values vary between 0.375–0.7 eV for LTO phases which are all named "spinel." This can be understood by the fact that some authors use the ideal stoichiometry $LiTi_2O_4$ of the mineral spinel ($MgAl_2O_4$) [10]. In this ideal spinel stoichiometry, the 16*d* sites are no longer shared between Li and Ti but fully occupied by Ti. Hence, there exists only one single diffusion path for Li between 8*a* sites. Other authors use indeed the actual stoichiometry $Li_4Ti_5O_{12}$, but they consider only a limited number of the possible diffusion paths [11]. In the actual stoichiometry, the diffusion paths of Li become nonequivalent due to the mixed occupation of the 16*d* sites. This leads to a variety of migration paths which have not been investigated by DFT simulations so far. Therefore, we have investigated in our DFT study on Li diffusion a connected network of possible paths for the correct stoichiometry of the two LTO phases $Li_4Ti_5O_{12}$ and $Li_7Ti_5O_{12}$, respectively. Moreover, the influence of Li^+_{16d} on nearby lithium diffusion paths is studied, and the question is addressed as to whether 16*d* sites actively take part in the Li migration processes.

In Sec. II, we will briefly present our model and the computational setup. The results will be shown in Sec. III, discussed in Sec. IV, and summarized in Sec. V.

*Benedikt.Ziebarth@iwm.fraunhofer.de

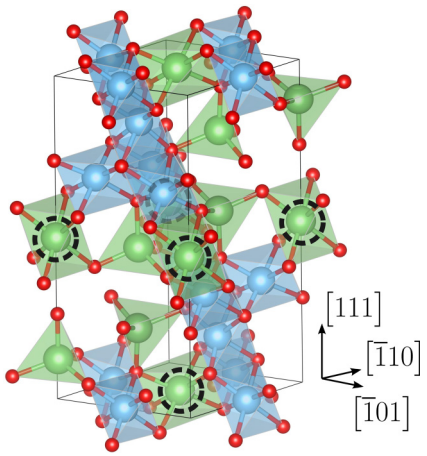

FIG. 1. (Color online) Hexagonal supercell of LTO in spinel phase with correct stoichiometry ($Li_8Ti_{10}O_{24}$). Red spheres are oxygen ions (32*e*), blue spheres are titanium ions (16*d*), and green spheres are lithium ions. Lithium ions on 16*d* sites are encircled; the remaining lithium ions occupy the 8*a* sites. The tripod indicates the directions in the cubic LTO structure by Miller indices [hkl].

II. MODEL SETUP

A. Structural model of $Li_{4+x}Ti_5O_{12}$

In order to achieve the correct stoichiometry of LTO and to keep the number of atoms as small as possible, a hexagonal supercell is constructed which contains two formula units of LTO, i.e., $Li_{8+2x}Ti_{10}O_{24}$, $0 \leqslant x \leqslant 3$. The z axis of this cell is chosen to be along the [111] direction of the fcc supercell. The degree of freedom in arranging Li^+_{16d} ions has been investigated by means of total-energy calculations. The most stable structure is found to have the largest possible distances between Li^+_{16d} ions (see Figs. 1 and 2). Every sixth layer along the z axis of this cell consists of lithium ions only. In the search for different orderings of Li^+_{16d} in the spinel phase, another structure was found which was similar in energy and showed a similar arrangement of atoms as the supercell which was used for further calculations: again, every sixth layer was occupied by lithium only and also the Li^+_{16d} which was not part of this Li-rich layer had the same distance to it. All other investigated structures were by about 0.4 to 4.3 eV (per $Li_8Ti_{10}O_{24}$) higher in energy. This search procedure was not applied to the rocksalt phase which can be obtained from the spinel phase by lithiation. During the lithiation, the titanium ions on 16*d* sites are immobile and hence the ordering of Li^+_{16d} is already determined by their ordering in the spinel phase. Finite-size effects are negligible since calculations with an orthorhombic supercell which is twice as large as the hexagonal supercell have not shown any significant difference. Please note that the sixth layer which consists of only Li atoms is possibly a result of our $T = 0$ K calculation as no superstructure of Li^+_{16d} ions is observed in x-ray diffraction experiments at finite temperature [7]. Inversion symmetry is still present in our model.

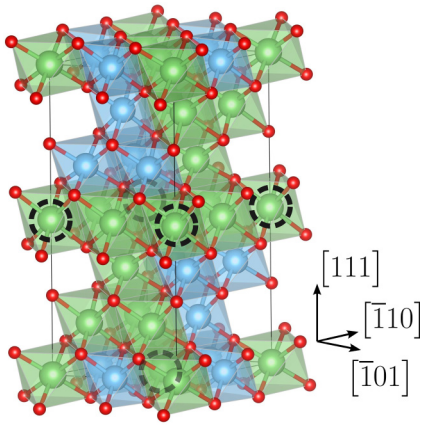

FIG. 2. (Color online) Hexagonal supercell of LTO in rocksalt phase with correct stoichiometry ($Li_{14}Ti_{10}O_{24}$). Red spheres are oxygen ions (32*e*), blue spheres are titanium ions (16*d*), and green spheres are lithium ions. Lithium ions on 16*d* sites are encircled; the remaining lithium ions occupy the 16*c* sites. The tripod indicates the directions in the cubic LTO structure by Miller indices [hkl].

B. Lithium vacancy diffusion

It is known from x-ray diffraction experiments that lithium ions occupy 8*a*, 16*c*, and 16*d* positions. Several possible diffusion paths in the material exist which are displayed in Fig. 3. 8*a* and 16*c* positions are alternatingly lined up, and paths do not directly connect two sites of the same type. As lithium ions rearrange between 8*a* and 16*c* positions upon lithiation, it is plausible to assume that lithium diffusion takes place mainly between those two positions. Furthermore, a lithium diffusion mechanism via vacancy hopping is assumed and, for this reason, there is only one Li vacancy per supercell.

Paths of Li vacancy migration in the supercell were chosen to ensure not only local jumps, but a connected network for long-range migration. In particular, we were interested in

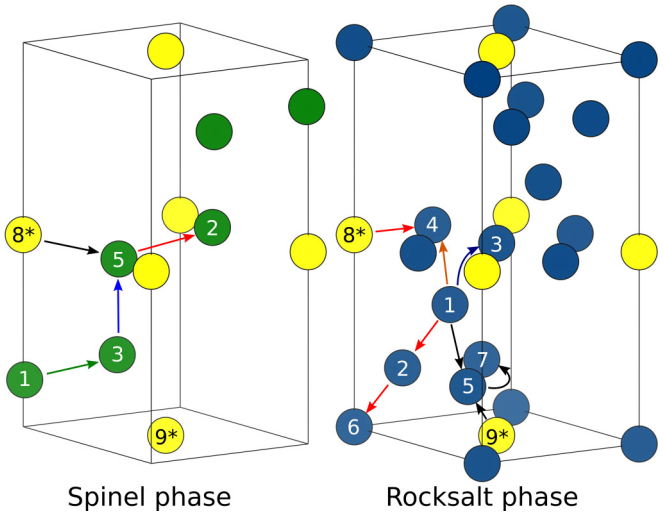

FIG. 3. (Color online) The investigated diffusion paths of lithium vacancies in the spinel and the rocksalt phases are depicted. Li ions on 8*a*, 16*c*, and 16*d* sites are colored green, blue, and yellow, respectively. Note that the spinel and rocksalt phases of LTO only differ by the occupation of 8*a* and 16*c* sites with Li atoms. 16*d* sites which are occupied by Li atoms are marked with an asterisk. The colors of the arrows indicating the paths coincide with the colors used in the following Figs. 4–6.

diffusion between 8*a* sites in the spinel phase and 16*c* sites in the rocksalt phase. Some additional paths between 16*d* sites and other sites were chosen in order to determine their role in the migration path network as well. The number of independent paths was reduced, taking mirror symmetry and inversion symmetry into account. For the identified diffusion paths, we calculated their activation energy barriers ΔE which are related to the defect jump rates Γ by an Arrhenius-type equation [12]

$$\Gamma = \nu e^{-\Delta E/k_B T},$$

where ν is the frequency factor, T is the absolute temperature, and k_B is the Boltzmann's constant. The change of the frequency factor within one material is assumed to be negligible with respect to the influence of the activation energy barrier. The energies of the intermediate and final states are the same within 0.03 eV for the hexagonal and for the twice as large orthorhombic supercells.

C. Computational methodology

All DFT calculations have been carried out using the QUANTUM ESPRESSO PWscf code [13] which uses a plane-wave basis to express the wave function of the valence electrons. Core electrons and the nuclei are described by ultrasoft pseudopotentials. The generalized gradient approximation in PBE parametrization was used for the exchange-correlation functional [14,15]. Energy cutoffs of 30 and 300 Ry for the plane-wave basis and electron density representation, respectively, were found to yield converged results. The Brillouin zone was sampled by a $4 \times 4 \times 4$ Monkhorst-Pack grid [16]. The lattice volume and atom positions were relaxed until the remaining force acting on the atoms was less than 10^{-4} eV/Å. The *minimum energy paths* (MEPs) for jumps of Li ions between sites were calculated using the *nudged elastic band* (NEB) method [17]. In addition, the *climbing image* NEB method was applied to ensure correct location of activation barriers [17]. The threshold for the total force, which is acting on the NEB images of the interpolated reaction path, was set to 0.05 eV/Å. The MEP was approximated by fitting a polynomial spline to the energies and energy gradients of the images.

III. RESULTS

A. Lithium vacancy diffusion in $Li_4Ti_5O_{12}$

For the spinel phase $Li_4Ti_5O_{12}$, four paths connecting five different lithium positions have been investigated (cf. Fig. 4). The shapes of the paths 1–3 and 3–5 are both asymmetric. The energy barriers for the paths $3 \rightarrow 5$ and $3 \rightarrow 1$ are roughly similar, while for the opposite directions the energy barrier for path $5 \rightarrow 3$ is by about 0.10 eV higher than the energy barrier for path $1 \rightarrow 3$.

As expected due to inversion symmetry, path 2–5 is perfectly symmetric. It crosses the lithium-rich layer and shows an activation barrier of 0.48 eV for both directions. The passed 16*c* site does not lead to a flat plateau or a (meta)stable transition state.

The path 8*–5 which connects 16*d* and 8*a* positions is very asymmetric, and the activation barrier for the lithium vacancy to move towards the 8*a* position is about 0.92 eV, whereas it is comparable with the activation barriers of other paths for the reverse direction. The passed 48*f* position on this path is noticeable by a flat plateau of the MEP.

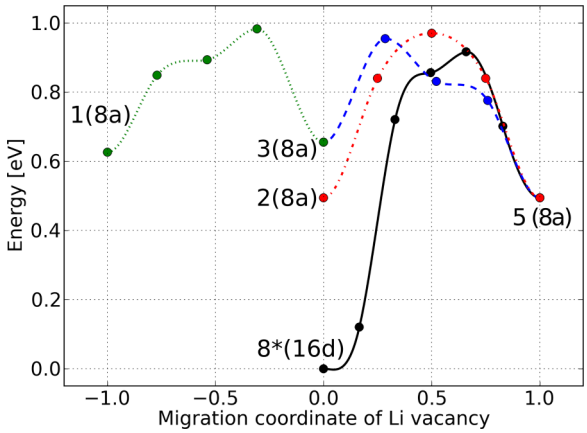

FIG. 4. (Color online) MEPS of all calculated paths in the spinel phase $Li_4Ti_5O_{12}$. The site labeled by an asterisk is a 16*d* site. Note that the migration coordinate of the lithium vacancy is drawn on the abscissa. The paths are discussed in the text.

If the energies of the stable positions are compared relative to each other, it is evident that the most stable site for a lithium vacancy is 16*d* (site 8*, cf. Fig. 4). The energetically closest configurations are about 0.49 eV higher in energy (sites 2 and 5). The next ones are additionally by about 0.15 eV higher in energy (sites 1 and 3).

B. Lithium vacancy diffusion in $Li_7Ti_5O_{12}$

For the rocksalt phase $Li_7Ti_5O_{12}$, the MEPs of eight paths have been calculated (cf. Fig. 5). The paths connecting two 16*c* positions passing an 8*a* site show activation barriers between 0.20 and 0.51 eV. The intermediate 8*a* position is an energy maximum and does not give evidence for a (meta)stable transition state.

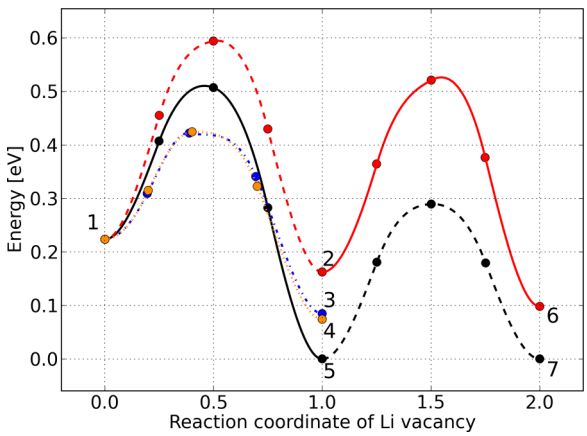

FIG. 5. (Color online) MEPs of all paths connecting two 16*c* sites in the rocksalt phase $Li_7Ti_5O_{12}$. Note that the migration coordinate of the lithium vacancy is drawn on the abscissa. The paths are discussed in the text.

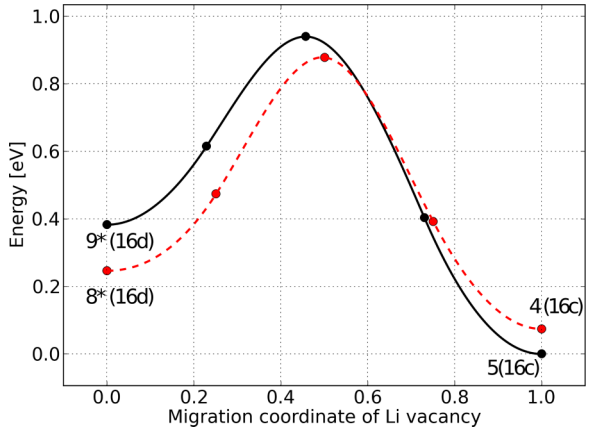

FIG. 6. (Color online) MEPs of paths connecting a 16*c* site with a 16*d* site in the rocksalt phase $Li_7Ti_5O_{12}$. The sites labeled by an asterisk are 16*d* sites. Note that the migration coordinate of the lithium vacancy is drawn on the abscissa. The absolute energy agrees with that of Fig. 5. The paths are discussed in the text.

Paths connecting 16*d* and 16*c* positions (Fig. 6) show very large energy barriers (0.80–0.94 eV) for lithium moving away from the 16*d* position, while for the reverse direction the energy barriers (0.56–0.63 eV) are comparable to the activation barriers of the 16*c*-16*c* paths (Fig. 5). While the energy landscapes of those paths are comparable, the geometric paths differ: for the 8*–4 path, the lithium motion takes place in the lithium-rich layer and the diffusion path lies between two tetrahedral 48*f* vacancies which are surrounded by lithium ions. In the 9*–5 path, the moving lithium occupies a 48*f* position at the intermediate state. This vacancy is surrounded not only by lithium ions, but also by titanium ions. In contrast to $Li_4Ti_5O_{12}$, no vacancy trapping on 16*d* sites is observed.

By looking at the energies of the different vacancy positions in Fig. 5, three groups of sites with similar energy can be identified: the first group consists of sites 1 and 2 and has an energy of about $E \approx 0.2$ eV; the second group is composed of sites 3, 4, and 6 and has an energy of about $E \approx 0.1$ eV; and sites 5 and 7 are forming the third group which has an energy of about $E \approx 0.0$ eV. In Fig. 6, the energy of the 16*d* site 8* is comparable to the first group, while the 16*d* site 9* has a larger energy of about 0.39 eV.

IV. DISCUSSION

In the following, the relative energies of the different vacancy positions will be discussed. In the spinel phase (cf. Fig. 4), the low energy of the vacancy at a 16*d* site is due to the longer bond length between oxygen and lithium in the octahedral coordination. In order to understand the energy of the different 8*a* sites, a neighbor analysis was carried out. All 8*a* sites are tetrahedrally coordinated by four oxygen atoms, therefore, the second-nearest neighbors are significant for the energy. The second-nearest neighbor shell has 16 atoms which consist of 5 8*a* and 11 16*d* sites. The 5 8*a* sites are fully occupied by lithium, whereas the 16*d* sites are shared between titanium and lithium. In addition, the tetrahedral volumes were determined to monitor the overlap repulsion behavior. The results in Table I show that there exists a correlation between the number of lithium neighbors and the tetrahedral volume as well as the energy, e.g., one can see that the position with the fewest lithium neighbors shows the largest volume and the highest energy of all studied positions. The correlation, however, does not follow an easy trend which would be caused by a single dominant mechanism such as Coulomb interaction or overlap repulsion. Thus, we believe that the observations originate from a competition of several mechanisms.

TABLE I. Vacancy energies, polyhedra volumes, and numbers of second-nearest neighbors for 8*a* sites in the spinel phase $Li_4Ti_5O_{12}$. Energies, volumes, and number of nearest neighbors for 16*d* sites are included for completeness.

Site			Neighbors	
(cf. Fig. 4)	Energy (eV)	Volume (Å^3)	Li	Ti
1 (8*a*)	0.63	4.02	6	10
2 (8*a*)	0.49	4.05	7	9
3 (8*a*)	0.65	4.27	5	11
5 (8*a*)	0.49	4.05	7	9
8* (16*d*)	0.0	12.27	6	6

In the rocksalt phase, the same neighbor analysis is carried out for the 16*c* sites (cf. Table II). Again, only the second-nearest-neighbor shell is of importance because the nearest-neighbor coordinations are all the same. In all cases, the second-nearest neighbor shell has 12 atoms which occupy 6 8*a* and 6 16*c* sites. Again, the 8*a* sites are fully occupied by lithium, while the 16*c* sites are shared between lithium and titanium. Also, in the case of rocksalt, the results in Table II show a correlation between the numbers of lithium neighbors and energy as well as octahedra volumes. Unlike in the spinel, we observe a relation between the number of lithium neighbors and the volume: more lithium neighbors yield a larger octahedra volume. The energy does not follow this tendency because the lowest energy is found for positions which are surrounded by seven lithium ions, while the largest energy is found for sites which are surrounded by six lithium ions. Sites with eight lithium neighbors show energies

TABLE II. Vacancy energies, polyhedra volumes, and numbers of second-nearest neighbors for 16*c* sites in the rocksalt phase $Li_7Ti_5O_{12}$. Energies, volumes, and number of nearest neighbors for 16*d* sites are included for completeness.

Site			Neighbors	
(cf. Figs. 5 and 6)	Energy (eV)	Volume (Å^3)	Li	Ti
1 (16*c*)	0.22	12.63	6	6
2 (16*c*)	0.16	12.56	6	6
3 (16*c*)	0.08	13.38	8	4
4 (16*c*)	0.07	13.35	8	4
5 (16*c*)	0.00	13.07	7	5
6 (16*c*)	0.10	13.14	8	4
7 (16*c*)	0.00	13.07	7	5
8* (16*d*)	0.25	12.21	6	6
9* (16*d*)	0.38	12.03	6	6

TABLE III. Summary of all calculated energy barriers for lithium diffusion in LTO in the spinel phase and the rocksalt phase.

		Energy barriers	
LTO phase	Diffusion path	$E_{\rightarrow}$ (eV)	$E_{\leftarrow}$ (eV)
$Li_4Ti_5O_{12}$	$1 \leftrightarrow 3$	0.36	0.33
	$3 \leftrightarrow 5$	0.30	0.46
	$5 \leftrightarrow 2$	0.48	0.48
	$8^* \leftrightarrow 5$	0.92	0.42
$Li_7Ti_5O_{12}$	$1 \leftrightarrow 2$	0.37	0.43
	$1 \leftrightarrow 3$	0.20	0.34
	$1 \leftrightarrow 4$	0.20	0.35
	$1 \leftrightarrow 5$	0.28	0.51
	$5 \leftrightarrow 7$	0.29	0.29
	$2 \leftrightarrow 6$	0.36	0.42
	$8^* \leftrightarrow 4$	0.63	0.80
	$9^* \leftrightarrow 5$	0.56	0.94

in-between. Such a behavior can again only be understood by at least two counteracting mechanisms such as Coulomb interaction and overlap repulsion and can not be described within a simplified explanation.

The results from the above energy analysis of the lithium vacancies in LTO suggest that 16*d* positions may trap lithium vacancies in $Li_4Ti_5O_{12}$ but remain filled with lithium ions in $Li_7Ti_5O_{12}$. Since the activation barrier of paths connecting 16*d* with 16*c* (in $Li_7Ti_5O_{12}$) or 8*a* positions (in $Li_4Ti_5O_{12}$) is very large (>0.80 eV), diffusion processes involving 16*d* sites take place on a longer time scale. This assumption is supported by NMR experiments of Wagemaker *et al.* [5] in which no evidence was found for mobile Li^+_{16d} in $Li_4Ti_5O_{12}$.

The calculated energy barriers for the MEPs in the spinel phase and the rocksalt phase are summarized in Table III. In the results about vacancy diffusion in the spinel phase, the paths 1–3 and 3–5 showed an asymmetric behavior. In order to explain this behavior, the coordination of oxygen atoms has been analyzed. In the perfect spinel phase ($Li_1Ti_2O_4$), all oxygen atoms would be coordinated by three titanium ions and one lithium ion. For the actual stoichiometry, this is no longer the case because some of the 16*d* sites are occupied by lithium. Therefore, some oxygen ions are coordinated by two lithium ions and two titanium ions, whereas all other oxygen ions are coordinated by three titanium ions and one lithium ion. Oxygen ions of the first kind will be denoted by (a)-oxygen, while for the latter case they are denoted by (b)-oxygen (cf. Fig. 7).

Please note that the NEB paths describe the motion of a lithium vacancy while we look at the position of the moving lithium ion in the following. We analyze the face spanning oxygen atoms on the paths 1–3 and 3–5 (cf. Fig. 8) and also calculate the area of the face while a lithium ion is passing it. This is depicted in Fig. 8: for path 1–3 the face at site 3 is spanned by one oxygen ion of type (a) and two of type (b) (4.77 Å^2), the face at site 1 is spanned by two oxygen ions of type (a) and one of type (b) (4.53 Å^2). For path 3–5, the face at site 3 is spanned by three oxygen atoms of type (b) (4.73 Å^2), while the face at site 5 is spanned by 3 (a)-type oxygen ions (4.43 Å^2). One can see that the face area is correlated to the

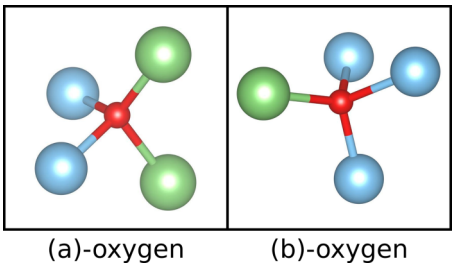

FIG. 7. (Color online) In $Li_4Ti_5O_{12}$, there exist two differently coordinated oxygen atoms in each phase: oxygen coordinated by two lithium ions and two titanium ions is denoted by (a)-oxygen, and oxygen coordinated by one lithium ion and three titanium ions is denoted by (b)-oxygen. Oxygen atoms are red, titanium atoms are blue, and lithium atoms are green.

oxygen which span the triangle, e.g., the smallest area of a face is obtained for a triangle spanned by three (a)-oxygen. The correlation, however, does not follow a simple trend because the area of triangle spanned by three (b)-oxygen is by about 0.04 Å^2 smaller than a triangle spanned by two (b)-oxygen and one (a)-oxygen. Nevertheless, this difference in the area of the faces spanned by the oxygen atoms can very nicely explain the asymmetry of the Li diffusion path due to increased overlap repulsion of the Li when crossing the smaller faces.

From the above discussion, it is obvious that neither the energy of lithium vacancies in spinel nor the energy landscape of diffusion paths of lithium ions in spinel can be described with a simplified model.

In order to estimate the ratio of the time scales on which the diffusion in the two different phases take place, we choose the time-limiting diffusion process of both phases: the diffusion of a lithium vacancy from a 16*d* site to an 8*a* site in the spinel phase has a barrier of $\Delta E_{\text{spinel}} = 0.92$ eV. 16*d* sites in spinel act as a trapping site for lithium vacancies. However, if this trapping mechanism is saturated, the 16*d* sites can be excluded from the diffusion process and then one ends up with an energy barrier between 8*a* sites of about 0.48 eV. In the rocksalt phase, the 16*d* sites repel the lithium vacancy and can therefore be neglected. Also, the vacancy jump between the

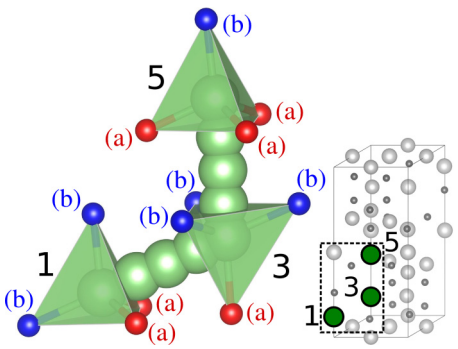

FIG. 8. (Color online) The MEPs from sites 1 to 3 and from sites 3 to 5 in $Li_4Ti_5O_{12}$ are shown. The green spheres indicating a lithium ion moving from sites 1 to 3 and from sites 3 to 5 (cf. Fig. 4). The red spheres are (a)-oxygen and the dark blue spheres are (b)-oxygen. The energy landscape of these paths is asymmetric as shown in Fig. 4 and discussed in detail in the text.

sites 1 and 5 is not necessary for the diffusion of Li throughout the crystal, hence, we are left with the next lower energy barrier of $\Delta E_{\text{rocksalt}} = 0.43$ eV for the path 1–2 in rocksalt. By assuming the frequency factor in the spinel and rocksalt to be the same, we can estimate the ratio between the defect jump rates at room temperature by

$$\rho = \frac{\Gamma_{\text{spinel}}}{\Gamma_{\text{rocksalt}}} = \frac{\nu e^{-\Delta E_{\text{spinel}}/k_B T}}{\nu e^{-\Delta E_{\text{rocksalt}}/k_B T}}.$$

We find $\rho = 5 \times 10^{-9}$ when the 16*d* sites in spinel are included. This clearly shows the property of these sites to trap vacancies. When neglecting them, we get $\rho = 0.142$ which suggests that at room temperature the Li diffusion efficiency of the rocksalt phase is by about one order of magnitude higher than that of the spinel phase.

Similar theoretical calculations of activation energies have been performed for $Li_{1+x}Ti_2O_4$ by Bhattacharya and Van der Ven [10]. Since all 16*d* positions in $Li_{1+x}Ti_2O_4$ are occupied by titanium, all 8*a* and all 16*c* sites are equivalent and no 16*d* site takes part in any diffusion event. For $Li_{\frac{7}{8}}Ti_2O_4$, the calculated activation barrier was about 0.375 eV. The activation barrier increased up to 0.5 eV for $Li_{\frac{1}{8}}Ti_2O_4$. These activation barriers compare well with those from our calculations. However, it has to be pointed out that most of our MEPs have an asymmetric shape, which in one case results in two different energy barriers for backwards and forwards jumps. Bhattacharya and Van der Ven did not find any evidence for a metastable 16*c* position in an 8*a* to 8*a* diffusion process in the spinel phase [10]. Interestingly, most paths calculated in our work show evidence of at least a flat plateau close to the 16*c* site. In addition, for the rocksalt phase $Li_2Ti_2O_4$, Bhattacharya and Van der Ven showed that the MEP connecting two 16*c* positions has an activation barrier of about 0.28 eV with an 8*a* position being a metastable transition state [10]. In our calculated MEPs, the transition state at the 8*a* site was always unstable. Again, the activation barrier compares well to our findings, but the shape of the MEP does not. This indicates that the missing 16*d* lithium ions and hence the different charge of the titanium ions may affect the relative energy of the 8*a* positions in the $Li_2Ti_2O_4$ composition.

Another theoretical study was performed by Chen *et al.* [11]: $Li_4Ti_5O_{12}$ was studied in a supercell of $1 \times 1 \times 3$ fcc supercells. Only one 8*a* to 8*a* path was calculated and no specific comments on the effect of Li^+_{16d} ions were made. As in the calculation of Bhattacharya and Van der Ven [10], no metastable 16*c* position was found. However, the calculated activation barrier was about 0.7 eV, which is almost twice as much as those found by Bhattacharya and Van der Ven [10] and found in our study. Furthermore, Chen *et al.* reported that for the rocksalt phase $Li_7Ti_5O_{12}$, the activation barrier of the MEP connecting two 16*c* positions is only 0.04 eV with a stable 8*a* position which is stabilized by an activation barrier of about 0.35 eV which is also in disagreement to the findings in our study.

In 2006, Wilkening *et al.* carried out *nuclear magnetic resonance* (NMR) measurements of energy barriers for lithium diffusion [4,18]. Energy barriers of about 0.76(2) and 0.41(3) eV were reported for $Li_4Ti_5O_{12}$ and $Li_{5.7}Ti_5O_{12}$, respectively. The measurements of the activation barriers were performed at temperature ranges of 300–410 K for $Li_4Ti_5O_{12}$ and 190–350 K for $Li_{5.7}Ti_5O_{12}$. The measured energy barrier in $Li_4Ti_5O_{12}$ is close to the calculations by Chen *et al.*, however, Wagemaker *et al.* [5] mentioned that fitting the measured data of $Li_4Ti_5O_{12}$ in a lower-temperature range of 300–350 K may yield an energy barrier of about 0.41 eV which agrees with the findings of Van der Ven [10] and with our findings.

Furthermore, Wagemaker *et al.* reported activation energies of about 0.31 ± 0.01 eV for hopping between 8*a* positions and 0.3 ± 0.1 eV for hopping between 16*c* positions in $Li_{4.3}Ti_5O_{12}$, $Li_5Ti_5O_{12}$, and $Li_6Ti_5O_{12}$ measured by NMR [5] in a temperature range of 148–473 K.

Recent NMR measurements performed by Hain *et al.* on $Li_4Ti_5O_{12}$ [6] showed energy barriers of about 0.55 ± 0.01 eV for $Li_4Ti_5O_{12}$, 0.39 ± 0.02 eV for $Li_6Ti_5O_{12}$, and 0.45 ± 0.02 eV for $Li_7Ti_5O_{12}$. These findings are a bit lower than those by Wilkening *et al.* However, Hain *et al.* measured the energy barriers in a larger temperature range of about 298–673 K.

Laumann *et al.* carried out neutron diffraction measurements on lithium migration at high temperatures in $Li_4Ti_5O_{12}$ [9]. They observed a strong increase of the volume of tetrahedral 8*a* sites with temperature. In addition, they reported that only 86% of the 8*a* sites remained occupied by lithium at 900 °C. This was attributed to anharmonic motions and migration of lithium to other sites. It was shown that some of the lithium ions move from 8*a* sites to empty 32*e* sites which are supposed to be metastable. Furthermore, a one-particle potential with the following energy barriers was derived: $8a \rightarrow 32e$ (0.5 eV), $32e \rightarrow 8a$ (0.2 eV), $32e \rightarrow 16c$ (0.5 eV). In our calculations, these 32*e* sites are not (meta)stable for Li possibly due to the overlap repulsion between the face spanning oxygen and lithium. The observed strong volume increase of the tetrahedral 8*a* sites with temperature may reduce the ionic overlap repulsion such that this face-centered site becomes (meta)stable. If we assume that the 32*e* positions are unstable, the effective energy barrier for 8*a* to 8*a* diffusion over 16*c* sites becomes 0.8 eV at 900 °C. This energy barrier value is very different from that of our work which was calculated for 0 K. The large difference might be as well due to other anharmonic effects at such high temperatures. A comparison of results is therefore not straightforward due to the different temperatures.

Another high-temperature study on $Li_4Ti_5O_{12}$ was performed by Vijayakumar *et al.* [8] who carried out ^{6}Li magic angle spinning nuclear magnetic resonance measurements and molecular dynamics simulations with empirical interatomic potentials. In contrast to Laumann *et al.*, they observed that Li partially relocates from 8*a* sites to 16*c* sites for temperatures higher than 600 K. This relocation leads to a large number of lithium vacancies at 8*a* sites which enhances the Li diffusion via jumps between 16*c* sites through vacant 8*a* sites. Li atoms on 16*d* sites remain inactive in all calculations and measurements.

The activation barriers found in the experiments mentioned above show the tendency that they are slightly higher for the spinel phase than for the rocksalt phase which is in agreement with our findings. Also, the heights of the measured and calculated activation barriers agree roughly. The comparison between our results and the results for compositions between the spinel and the rocksalt phase is quite difficult: assuming mainly bulk diffusion of lithium ions and a phase coexistence

between the spinel and rocksalt phases would suggest that the activation barrier is a superposition of energy barriers in the spinel and rocksalt phases. Therefore, a linear dependence on the lithium concentration is expected, but this is not found. Instead, a lower activation energy for intermediate lithium concentrations is observed which indicates that an additional diffusion mechanism is important such as diffusion along interfaces. In this concentration regime, many Li vacancies are present, close to each other, and therefore interacting. This can have a significant effect on migration barriers of Li ions. But, this effect is not taken into account in our study, which is based on the assumption of single, noninteracting Li vacancies (i.e., one per supercell, cf. Figs. 1 and 2) as a mechanism for Li diffusion. Our model could be adopted for this complication, but this may be left for a further investigation. Alternatively, the lithium diffusion process for compositions between the spinel and the rocksalt phases could also be dominated by a solid solution at high temperatures.

V. CONCLUSION

LTO is a promising anode material for future battery generations. In this work, we studied the lithium diffusivity in the spinel and rocksalt phases by means of NEB calculations based on DFT. In particular, we investigated the influence of the mixed occupation of 16*d* positions by lithium ions and titanium ions on the lithium diffusion. The influence on the activation energy barriers can be of about the same order of magnitude as the activation barrier itself, and therefore it is not negligible for calculations of diffusion constants. In the spinel phase, the activation barriers for hopping between 8*a* positions are in the range of 0.30–0.48 eV. Interestingly we find that the formation of Vac_{16d,Li^+} is very likely. This can explain the low lithium diffusivity in pure $Li_4Ti_5O_{12}$ observed in NMR experiments because it results in vacancy trapping.

For the rocksalt phase, the calculated activation energy barriers for paths connecting 16*c* positions are in the range of 0.20–0.51 eV. Unlike in the case of the spinel phase, Li^+_{16d} ions remain on their positions as reported by Wagemaker *et al.* [5].

Moreover, for both the spinel and the rocksalt phases, the shapes of the MEPs are affected by the mixed occupancy and can even become asymmetric in some cases. The relative energies of lithium vacancies at different positions are affected by their local environment.

Due to the variety of energy barriers even within one of the end members of LTO ($Li_{4x}Ti_5O_{12}$ with $x = 0$ or 3), diffusion constants can not be obtained reliably using simplified models and hence must be calculated using numerical simulation methods such as kinetic Monte Carlo (kMC) which is capable to take the different energy barriers into account.

ACKNOWLEDGMENT

This work was funded by the German Federal Ministry of Education and Research BMBF within the Project HE-Lion (Grant No. INLB03088008).

[1] S. Scharner, W. Weppner, and P. Schmid-Beurmann, J. Electrochem. Soc. **146**, 857 (1999).
[2] A. Deschanvres, B. Raveau, and Z. Sekkal, Mater. Res. Bull. **6**, 699 (1971).
[3] K. Persson, V. Sethuraman, L. Hardwick, Y. Hinuma, Y. Meng, A. van der Ven, V. Srinivasan, R. Kostecki, and G. Ceder, J. Phys. Chem. Lett. **1**, 1176 (2010).
[4] M. Wilkening, W. Iwaniak, J. Heine, V. Epp, A. Kleinert, G. Nuspl, W. Bensch, P. Heitjans *et al.*, Phys. Chem. Chem. Phys. **9**, 6199 (2007).
[5] M. Wagemaker, E. van Eck, A. Kentgens, and F. Mulder, J. Phys. Chem. B **113**, 224 (2008).
[6] H. Hain, M. Scheuermann, R. Heinzmann, L. Wünsche, H. Hahn, and S. Indris, Z. Anorg. Allg. Chem. **638**, 1581 (2012).
[7] M. Wagemaker, D. Simon, E. Kelder, J. Schoonman, C. Ringpfeil, U. Haake, D. Lützenkirchen-Hecht, R. Frahm, and F. Mulder, Adv. Mater. **18**, 3169 (2006).
[8] M. Vijayakumar, S. Kerisit, K. M. Rosso, S. D. Burton, J. A. Sears, Z. Yang, G. L. Graff, J. Liu, and J. Hu, J. Power Sources **196**, 2211 (2011).
[9] A. Laumann, H. Boysen, M. Bremholm, K. T. Fehr, M. Hoelzel, and M. Holzapfel, Chem. Mater. **23**, 2753 (2011).
[10] J. Bhattacharya and A. Van der Ven, Phys. Rev. B **81**, 104304 (2010).
[11] Y. Chen, C. Ouyang, L. Song, and Z. Sun, Electrochim. Acta **56**, 6084 (2011).
[12] G. H. Vineyard, J. Phys. Chem. Solids. **3**, 121 (1957).
[13] P. Giannozzi, S. Baroni, N. Bonini, M. Calandra, R. Car, C. Cavazzoni, D. Ceresoli, G. Chiarotti, M. Cococcioni, I. Dabo *et al.*, J. Phys.: Condens. Matter **21**, 395502 (2009).
[14] D. Vanderbilt, Phys. Rev. B **41**, 7892 (1990).
[15] J. P. Perdew, K. Burke, and M. Ernzerhof, Phys. Rev. Lett. **77**, 3865 (1996).
[16] H. Monkhorst and J. Pack, Phys. Rev. B **13**, 5188 (1976).
[17] G. Henkelman, B. Uberuaga, and H. Jónsson, J. Chem. Phys. **113**, 9901 (2000).
[18] M. Wilkening, R. Amade, W. Iwaniak, and P. Heitjans, Phys. Chem. Chem. Phys. **9**, 1239 (2007).